The optical error budget for the MRO Interferometer

INT-402-ENG-nnnn rev 0.2

David Buscher <dfb@mrao.cam.ac.uk>

Mar 13, 2007

Magdalena Ridge Observatory
New Mexico Tech
801 Leroy Place
Socorro, NM 87801,USA
Phone: (505)835-6431
Fax: (505)835-6807
http://www.mro.nmt.edu

1 Objectives

1. To describe the components of the array which degrade the interferometric signal-to-noise ratio and the allocations of this degradation to the different components.
2. To determine whether the science goal of fringe-tracking at H=14 is achievable within the current array design.

2 Summary

The goal of fringe-tracking at H=14 is achievable if the given error budget allocations are adhered to.

3 Introduction

By far the greatest limiting factor to accomplishing competitive interferometric science is being able to observe faint targets. This is primarily for 2 reasons:

1. The modest aperture sizes and short integration times imposed by atmospheric "seeing" on interferometers means that the number of photons collected per integration from a given astronomical target is orders of magnitude less for an interferometer than for a conventional telescope.
2. The interferometric light path inevitably includes a large number of components, each of which distorts the optical wavefront and scatters or absorbs photons, thereby further reducing the signal-to-noise ratio of the interferometric signal.

The first of these two effects cannot be alleviated except by going to sites with exceptional seeing or into space. For the MROI, we are limited to the characteristics of the available site. The second of these is under control of the interferometer designer, and can be alleviated by (a) using the minimum of optical components in the beam train, and (b) making sure that each component loses the least amount of signal as possible. In order to achieve the second of these aims, it is often possible to reduce the losses in each component by purchasing higher-performance components, but the components tend to cost exponentially more the tighter the tolerances are set, and achieving these tolerances is easier for some components than for others.

From this emerges the concept of an error budget, which assigns tolerances to different components in a way which does not place impossible demands on any single component but achieves the overall best performance. For the MROI there are a large number of such components so the error budget has many contributing factors. This document serves to identify all these contributing factors in the current design and to assign a realistically-achievable requirements on the performance for each component. Only requirements which directly affect the optical performance of the system are considered, and not, for example, requirements which determine how fast the system can acquire data etc.

The error budgets are calculated on a spreadsheet which gives details of all the components. These details could not all fit in this document and so the reader is referred to the spreadsheet for greater insight.

4 Top-level system performance goals

We can view the interferometer optical system of the MROI schematically as a block diagram as shown in Figure 1.

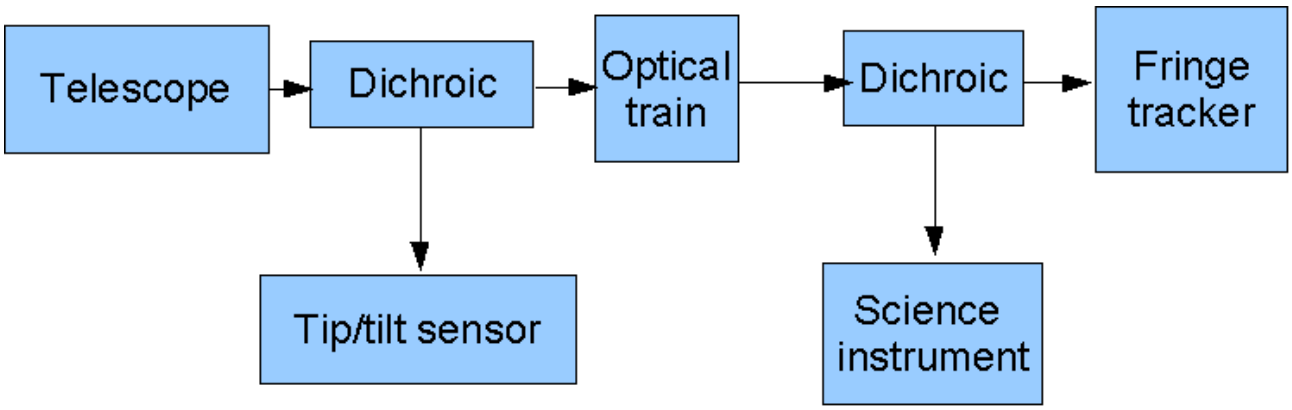

Figure 1: Block diagram of the interferometer optical system

It can be seen that the system has a single input but multiple outputs. For the majority of this document we will concentrate on a only one of output, namely the fringe tracker, but the principles of the analysis are similar for all the outputs. We concentrate on the fringe tracker because it is the system for which it is most difficult to meet the performance requirements required for the science. The most likely cause for not being able to do any science at all on an object will be if the object is too faint to drive the fringe tracker.

For the fringe tracker, the main performance requirement is the fringe-tracking signal-to-noise ratio (SNR). This can be defined in multiple ways, but for a group-delay fringe tracker operating at near its sensitivity limit, i.e. just on the edge of being able to track fringes at all, the SNR is given approximately by

$$SNR=(0.5V)^2 N_s^2 / (N_t^2+2N_t n\sigma^2+2n^2\sigma^4)^{1/2}$$

Where V is the RMS fringe contrast, N_s is the mean number of photons that would be detected from the target in a single coherent integration time in the absence of any background photons ("signal photons"), N_t is the mean number of photons detected in a single coherent integration time including all background photons ("total photons"), σ is the detector readout noise when reading a single pixel, and n is the number of pixel readouts per fringe estimate. Note that (a) the definition of V here is identical to the fringe contrast in the case of a 2-telescope interferometer – earlier versions of this formula had the 0.5 factor absorbed into the definition of V and (b) this formula is different from that used in the 2002 System Design Document: extra noise terms have been added consistent with the formula derived by Thorsteinsson (2004).

The SNR therefore depends on four main quantities, fringe contrast, the number of detected photons from the source, the number of background photons, and the read noise. We examine each in turn in the following sections, breaking the error budget down further for each term. We evaluate these quantities in the H and K bands, which are the main operating bands for the fringe tracker.

5 Photon throughput

For a source of a given brightness, the photon throughput simply determines what fraction of the photons which could be collected by each telescope that are detected by fringe tracking detector. Photons are lost through four major processes:

1. Atmospheric absorption and scattering
2. Surface and internal losses in optical components
3. Diffraction of light out of the beam train
4. Dead-time losses

5. Detector quantum efficiency

We discuss each of these processes in the following sections.

5.1 Atmospheric absorption and scattering

These are dependent on the amount of atmosphere that the light has to traverse, plus the composition of the atmosphere, particularly water vapor, particulates, and aerosols. We take values estimated for a lower-altitude site, Paranal in Chile, which are 0.97 in H band and 0.90 in the K-band.

5.2 Optical component losses

Each optical component in the beam train absorbs or scatters light. For each type of component we have assumed a certain amount of loss as shown in Table 1. These figures are reduced below their theoretical values by amounts of about one percent to account for additional scattering due to contaminants such as dust, and in the case of the telescope primary, to account for aging of the surface. It has been assumed that the transmissions of the components do not vary significantly between the H and K bands.

Surface	*Theoretical*	*Assumed*	*Number*	*Factor*
Aluminium	0.970	0.930	1	0.930
AR - BB	0.990	0.980	13	0.769
AR - BB int	0.990	0.990	7	0.932
CentralObscuration	0.900	0.900	1	0.900
Detector	0.650	0.650	1	0.650
Dichroic - dielectric	0.990	0.980	3	0.941
Infrasil 10mm	0.995	0.995	8	0.961
Infrasil20mm	0.990	0.990	7	0.932
Internal contact	0.995	0.995	3	0.985
Pixelcoupling	0.950	0.950	1	0.950
Silver	0.985	0.970	17	0.596
Splitter	0.990	0.980	2	0.960
			64	0.176

Table 1: Assumed values and calculated throughputs in the H and K bands for different types of optical components and their coatings. The number of each type of coating/substrate and their contribution to the total throughput is also shown.

It can be seen that the losses are dominated by the two most common surface coatings: the broadband anti-reflection coatings (AR-BB and AR-BB int – the latter are surfaces inside dewars which are assumed to be kept free of dust) of which there are 20 in total, and the silver mirror coatings, of which there are 17. The details of where these components are in the subsystems is shown in the accompanying spreadsheet.

The "pixelcoupling" item accounts for the imperfect coupling of light from the fringe tracker spectrograph onto the line of detector pixels. The "centralobscuration" item refers to the optical obscuration in the telescope due to the secondary and tertiary mirrors and spiders. This is specified as a 5% obscuration, but because of diffraction an extra 5% is lost

by the time the beam reaches the beam-combining area.

5.3 Diffraction

Photon losses due to diffraction along the optical train are calculated assuming:

1. D/r0 values of 2.4 and 1.7 at H and K respectively
2. A 95mm beam emerging from the telescopes
3. A 125mm aperture on the delay line, 400m from the telescopes
4. A nominal beam diameter of 13mm emerging from the beam compressors
5. A clear aperture of 18mm in the beam combiners, 20m from the beam compressors

The losses are shown in the summary table.

5.4 Dead-time

Losses due to dead-time are assumed to be 1% corresponding to a 300 microsecond readout and modulator stepping overhead in a 30 millisecond integration.

5.5 Summary

Table 2 shows the overall transmission of the system. It can be seen that this is significantly below the original goal of 20%, which was based on an estimate of 20 surfaces with a reflection of 95% per surface, which significantly undercounted the effects of the transmissive components in the system. This indicates the importance of minimizing the number of surfaces in the system.

	H	*K*
Atmospheric transparency	0.97	0.9
Reflection/transmission losses	0.18	0.18
Diffraction losses	0.78	0.77
Deadtime	0.99	0.99
System throughput product	0.13	0.12

Table 2: The overall throughput budget for MROI

6 Visibility losses

Almost everything in the optical system can contribute to the mismatch of the optical wavefronts from 2 telescopes and therefore contribute to visibility losses. We enumerate these effects below.

6.1 Spatial wavefront errors

Deviations of the wavefronts from the ideal flat wavefronts can be decomposed into Zernike polynomials of different orders. We treat separately the lowest order polynomials, corresponding to "piston" and "tip/tilt" and treat all higher order wavefront errors (WFE) as a third category. Static piston errors give rise to no visibility losses (assuming they are small with respect to the temporal coherence length of the light, which is several microns in the worst case), while temporally-changing piston errors give rise to "fringe smearing" and are treated separately. Tip and tilt errors are not properties of individual mirrors but of their alignment with respect to one another.

6.1.1 High-order WFEs

Higher order WFEs arise from atmospheric seeing and from instrumental errors. In both cases, the loss in visibility for a differential RMS wavefront error of σ radians between two wavefronts is given by $\exp(-\sigma^2/2)$, so that for two uncorrelated wavefronts each with error σ the visibility loss is $\exp(-\sigma^2)$. For a tip/tilted corrected atmospheric wavefront the wavefront variance goes as $0.134(D/r0)^{5/3}$ and this is reflected in Table 6 below.

Diffraction along the optical train has the effect of improving the visibility by rejecting the "bad" light, and this is calculated for the same system geometry as used in calculating the photon losses.

For instrumental WFEs we have tabulated every optical surface in the system and assigned a corresponding wavefront error. It has been assumed that larger optical surfaces are harder to polish than smaller surfaces, and that curved surfaces are harder to polish correctly than flat ones. Each surface is then assigned a required wavefront quality which is either $\lambda/10$ or $\lambda/20$ peak-to-valley when measured at a 633nm (HeNe laser) test wavelength. It is assumed that the RMS wavefront error is a factor of 5 below this (experimental measurements by Porro et al suggest that a factor of 5.5 is appropriate but we are being conservative here). The resulting wavefront errors are therefore either 13nm or 26nm, except for the UT optics which have a requirement for 42nm RMS for the primary and secondary combined. In addition, all the larger (>8 inch) optics have errors associated with supporting the optics and the curved optics have errors associated with aligning their optical axes. A total wavefront error of 99nm is calculated, i.e. about 1/16 wave at 1600nm.

6.1.2 Tilts

For an RMS tilt in each beam train of θ radians, the mismatch between the two interfering wavefronts leads to a visibility loss of $1-(\theta D/\lambda)^2/4$ where D is the diameter of the beams (this assumes that the tilt errors in the two beam trains are uncorrelated). We can see that it is the tilt in terms of the diffraction-limited angular resolution λ/D which is important. Magnifying or demagnifying the beam has a corresponding opposite effect on demagnifying or magnifying the allowable tilt variation, so allowable tilts can be compared in terms of their (de)magnified effect on the sky.

Rapidly and slowly-varying tilts have the same effect on the RMS visibility, so the error budgets for both static (alignment) errors and dynamic (drift/jitter) errors have been combined into a single table. Transmissive components do not affect beam tilt to first order and so have been excluded from the calculations. The allowed values are shown in Table 3 where it should be noted that the tilt errors are allowable two-axis errors i.e. the quadrature sum of the tip and tilt errors. There is only one alignment error for the entire system as the alignment system is assumed to measure the net effect of all mirrors and correct for this.

Item	Rms tilt (arcsec on sky)	Wavefront tilt (arcsec)
Uncorrected telescope jitter	0.0361	0.0361
M4	0.0149	0.2202
M5	0.0149	0.2202
Delay line	0.0149	0.2202
Beam compressor	0.0149	0.2202
Switchyard M1	0.0149	1.6095
Switchyard M2	0.0149	1.6095
Alignment errors	0.0149	1.6095
	0.0535	

Table 3: RMS two axis tip/tilt error budget. Both static and dynamic terms are included.

6.1.3 Pupil shear

The visibility loss due to a differential shear between beams of 1.4% of the beam diameter leads to a visibility loss of approximately 1%, thus an RMS pupil shear in each arm of 1% leads to a 1% visibility loss if the shears are uncorrelated. The shear error budget in the table below includes terms due to manufacturing errors, alignment and drift after alignment.

Item	RMS pupil shear (mm)	Pupil diameter (mm)	Fractional shear
Telescope manufacture	0.500	95.000	0.005
Alignment: telescope inner axis to beam train	0.500	95.000	0.005
Alignment: M5 to delay line shear reference	0.500	95.000	0.005
Delay line	1.000	95.000	0.011
Drift: M4/M5	1.000	95.000	0.011
Alignment error: switchyard	0.065	13.000	0.005
Drift: switchyard	0.043	13.000	0.003
Grand total			0.018

Table 4: Lateral pupil shear error budget for MROI

6.1.4 Piston jitter

Vibration of mirrors and atmospheric temporal variations are the two contributors to short-term piston jitter. If the amount of jitter that occurs during an exposure time in each arm is σ radians then the visibility reduction is given by $\exp(-\sigma^2)$. The instrumental jitter values are given in the Table below.

System	RMS piston vibration (nm)	Visibility loss
UT vibrations	57	0.951
UT tilt-piston coupling	57	0.951
M4	20	0.994
M5	20	0.994
Delay line	41	0.974
M10	20	0.994
Switchyard1	20	0.994
Switchyard2	20	0.994
Combiner	20	0.994
Grand total	102.85	0.85

Table 5: Instrumental piston jitter error budget

6.1.5 Group delay errors

The simulations of the group delay fringe tracker on which the fringe tracker limiting magnitudes are calculated implicitly include all the group delay errors caused by imperfect fringe tracking and so the visibility losses due to group delay errors are not included in this calculation. The group delay errors would have to be included in calculations for the science instrument.

6.1.6 Higher order dispersion errors

Differential optical dispersion in the two arms of an interferometer due to differential air or glass paths cause a combination of group delay (phase linear with optical frequency) and higher order wavelength-dependent errors. These quadratic and higher errors we designate as higher order errors and assign a total value of 1% fringe visibility loss to. A tolerance of 0.1mm on glass thickness is easily sufficient to reduce the visibility these higher order errors to a small fraction of this value.

6.1.7 Summary

Factor	Value	Units	H	K
Atmospheric high order WFE			0.559	0.717
Diffraction "fresnel filtering" gain			1.225	1.160
Instrumental high order static WFE	99.1514	nm	0.865	0.920
Uncorrected atmospheric tilt	0.0484	arcsec on sky	0.900	0.943
Instrumental tilt	0.0535	arcsec on sky	0.878	0.930
Pupil shear	0.0185		0.982	0.982
Atmospheric piston jitter (2t0 integration)			0.790	0.790
Instrumental piston jitter	102.8543	nm	0.855	0.914
Group delay errors			1.000	1.000
High-order dispersion effects			0.990	0.990
Differential polarisation effects			0.990	0.990
System visibility product			0.304	0.466

Table 6: Summary of visibility losses in the MROI

7 Thermal and sky background

We assume that the combination of the telescope, sky background and all the warm optics in the beam train emits as a blackbody at approximately 300K. A 300K blackbody source emits 3.66×10^{15} photons/second/sr/m^2 over the K bandpass (2.04-2.37 microns). For a system incorporating a cold pupil stop of diameter D and a cold pinhole which is exactly matched to the first Airy ring of the diffraction limited spot corresponding that pupil, the product of the solid angle and the area is given by $\pi (1.22\lambda/D)^2 \pi (D/2)^2 = 3.01\lambda^2$. For λ=2.1 microns, this translates to 49 thermal background photons per millisecond per cold stop in the system, of which there are 2 per baseline. There will be some loss of these photons due to losses inside the dewar, plus the detector QE, which we take to be a factor 0.5.

The thermal background in the H band is a factor 300 lower than in the K band. In this case background emission from the sky is dominant, and we take the sky background figures from the measured values in La Palma. Sky background losses are assumed identical to photon losses for the star, even though this is not strictly the case for diffraction losses.

8 SNR calculation

The goal for MROI is to be able to track fringes on sources as faint as H=14. Simulations have shown that a 5-spectral-channel group delay system can track fringes when the fringe-tracking SNR is as low as 0.33. Here we calculate the SNR for the observation of an H=14 and a K=14 object to compare with this value.

We make the following assumptions about the operating conditions.

Parameter	*Value*	*Units*
r0	0.14	m
lambda0	5.00E-07	m
windspeed	10	m/s
t0	4.40E-003	s
UT diameter	1.4	m
Integration time	2	t0

and we get the following values for the number of detected source and background photons.

Detected stellar flux per integration	*53.9*	*46.87*
Detected sky background flux	7.07	18.57
Thermal background per integration per cold stop	2.7	2615.91
Total noise photons	63.68	2681.36

We assume an 'ABCD' fringe detection scheme with 5 spectral channels, so 20 pixel reads in total per fringe tracking baseline per integration. This gives us the following values for the fringe-tracking SNR.

Read noise	*SNR at H*	*SNR at K*
0 Electrons	1.057	0.045
1 Electrons	0.782	0.044
1.5 Electrons	0.572	0.044
2 Electrons	0.409	0.043
3 Electrons	0.222	0.042
5 Electrons	0.089	0.037

As we can see we can meet the fringe tracking goals on an H=14 star, assuming a detector read noise of 2 electrons or better. The margin of safety for unaccounted-for effects is somewhat reduced from the calculation in the System Design Document of 2002. There a safety factor of greater than 2 was reached for the assumed value of the read noise of 1.5 electrons. However, the error budget here is based on much more detailed calculations and is far more realistic.